Observation of Quantum Jumps of a Single Quantum Dot Spin Using Submicrosecond Single-Shot Optical Readout

Aymeric Delteil, Wei-bo Gao, Parisa Fallahi, Javier Miguel-Sanchez, and Atac Imamoğlu
Institute of Quantum Electronics, ETH Zurich, CH-8093 Zurich, Switzerland
(Received 31 October 2013; published 19 March 2014)

Single-shot readout of individual qubits is typically the slowest process among the elementary single- and two-qubit operations required for quantum information processing. Here, we use resonance fluorescence from a single-electron charged quantum dot to read out the spin-qubit state in 800 nanoseconds with a fidelity exceeding 80%. Observation of the spin evolution on longer time scales reveals quantum jumps of the spin state: we use the experimentally determined waiting-time distribution to characterize the quantum jumps.

DOI: 10.1103/PhysRevLett.112.116802 PACS numbers: 73.21.La, 03.67.Lx, 42.50.-p

A fundamental difficulty in quantum information processing is the need for isolation of individual quantum systems from their noisy environment on the one hand, and the requirement for information extraction by selective coupling of qubits to classical (noisy) detectors on the other hand [1]. The requisite one- and two-qubit operations, as well as initialization of each qubit, can be carried out by using classical out-of-equilibrium external fields, such as lasers or microwaves; the lack of a need for heralding the successful completion of these operations ensures that they can be accomplished in short time scales. In contrast, quantum measurements are typically slow since information extraction by a classical observer is in many cases hindered by the need to protect the qubit from the external fluctuations. While ingenious schemes for fast qubit measurements have been developed, the time scales required for a high-fidelity qubit measurement remain at least an order of magnitude longer than those required for coherent operations in practically all quantum information processing schemes [2–4]. In the case of spin qubits in optically active quantum dots (QDs), the predicament is even more striking, since while optical excitation allows for fast turn on or off of light-matter interaction enabling spin readout, it at the same time allows for an additional fast channel for spin relaxation. In fact, with the exception of a slow coupled QD scheme requiring a designated readout QD [5], it has not been possible to carry out single-shot spin measurements on isolated optically active spin qubits [6].

In this Letter, we overcome the predicament underlying single-shot spin readout by enhancing the collection efficiency of resonance fluorescence (RF) from spin-dependent recycling transitions that are ubiquitous to single-electron charged QDs. The photon collection efficiency of 0.45% that we achieve allows us to obtain a single-shot spin readout fidelity exceeding 80% in a measurement time of 800 ns. This result corresponds to an enhancement of the spin readout time by almost three orders of magnitude as compared to the prior measurements on coupled QDs [5]. Continuous monitoring of the spin state enabled by single-shot readout reveals quantum jumps of the observed spin stemming either from the finite T_1 spin lifetime or spin pumping induced by the resonant readout laser. A theoretical analysis of quantum jumps using the waiting time distribution $[W(\tau)]$ was presented earlier [7,8]. Here we use the experimentally determined $W(\tau)$ and the second-order correlation function $[g^{(2)}(\tau)]$ of the RF events to characterize the (incoherent) spin dynamics.

Our experiment is carried out on a single InGaAs self-assembled quantum dot. The QD is placed in a low-quality factor ($Q < 10$) microcavity, consisting of a 28-layer distributed Bragg reflector mirror underneath the dot layer and a thin metal gate with a power reflectance $R < 0.5$ deposited on the top surface; this structure reduces the solid angle into which the QD photons are emitted. A solid immersion lens is mounted on the sample in order to further increase the extraction efficiency into a $NA = 0.65$ objective to 7.0% and the overall detection efficiency to ~0.45%. The semitransparent metallic top gate and a back n-doped layer form a Schottky diode structure, which is used to control the charge state of our quantum dot. The sample is in a liquid helium bath cryostat with an external magnetic field applied perpendicular to the growth direction (Faraday geometry). In this configuration, $|\uparrow\rangle \leftrightarrow |T_b\rangle$ and $|\downarrow\rangle \leftrightarrow |T_r\rangle$ are two transitions with strong oscillation strength, while the diagonal transitions $|\uparrow\rangle \leftrightarrow |T_r\rangle$ and $|\downarrow\rangle \leftrightarrow |T_b\rangle$ are only weakly allowed by the heavy-light hole mixing and have a ~450 weaker oscillation strength [Fig. 1(c)]. A confocal microscope is used to focus the excitation laser on the quantum dot as well as to collect photons from the quantum dot. In the excitation and collection arms, a cross-polarization technique [5,9] is used to suppress the reflected laser background by a factor $\sim 10^{-6}$. Scattered photons from the quantum dot are channeled to a superconducting single-photon detector (SSPD), and the detection events are analyzed using a time-correlated single photon counting module.

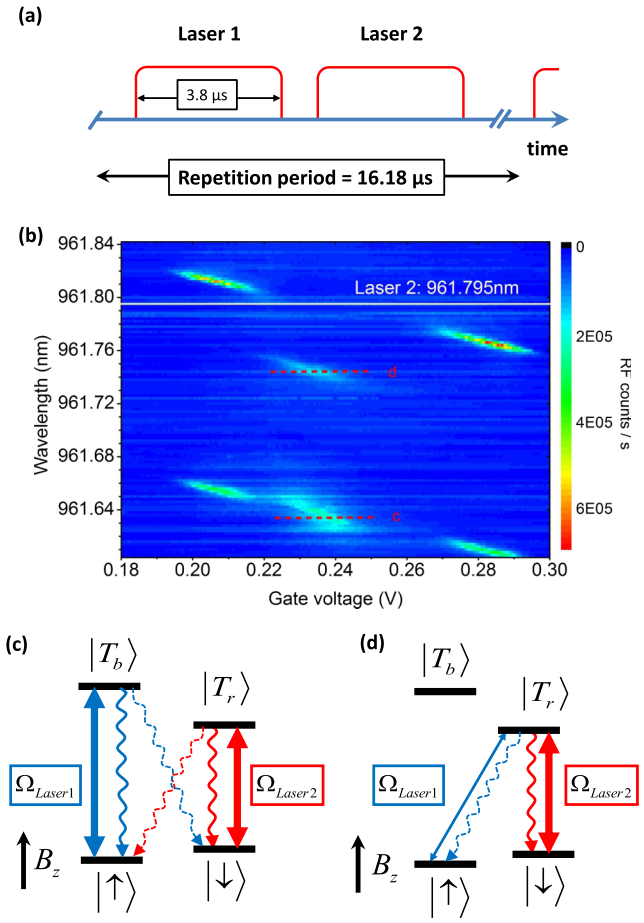

FIG. 1 (color online). (a) Pulse sequence used in the plateau scan as well as in the single-shot experiment. The two laser pulses have the same time duration. (b) The resonance fluorescence (RF) counts as a function of gate voltage and laser wavelength of laser 1. Here the RF counts include the total counts detected during both pulses. The magnetic field we use is 2 T and the wavelength of laser 2 is fixed at 961.795 nm. In the middle of the plateau, the signal disappears due to spin pumping except when the laser 1 wavelength is at 961.635 nm or 961.745 nm (marked with red lines) at a gate voltage ~0.236 V. At these two wavelengths, the corresponding energy level diagram is shown in (c) and (d), respectively.

To fully characterize the QD, we perform a two-color RF measurement in the single-electron charged regime using the pulse sequence shown in Fig. 1(a) at $B = 2T$. The two laser pulses with duration time 3.8 μs, separated by an interval of 0.5 μs, are generated from continuous-wave (cw) lasers using amplitude electro-optic modulators driven by two synchronized pulse pattern generators. We fix the wavelength of laser 2 to 961.795 nm and measure RF as a function of the gate voltage and the wavelength of laser 1 [Fig. 1(b)]. In the center of the plateau, the RF signal disappears due to spin pumping [10,11], with the exception of two particular wavelengths (marked with red lines c and d) where the signal is recovered due to spin repumping: in these two cases, at gate voltage $V = 0.235$ V, laser 2 is resonant with the red vertical transition, and laser 1 is resonant with either the blue vertical transition or the diagonal transition originating from $|\uparrow\rangle$, as shown in the corresponding energy level diagrams in Figs. 1(c) and 1(d). With the two successive pulses applied on the quantum dot, the spin is pumped back and forth between $|\uparrow\rangle$ and $|\downarrow\rangle$ states, ensuring that the RF signal is recovered. The different line shapes observed in Fig. 1(b) in these two cases are most likely due to dynamic nuclear spin polarization effects [12]. Using resonant cw excitation at zero magnetic field, we detect 2.6 million counts per second from the QD with excitation laser power above QD saturation. The trion lifetime is 0.65 ns; i.e. the QD emits $\sim 7.7 \times 10^8$ photons per second when driven well above saturation. Taking into account the effect of the ~90 ns dead time of our time-correlated single photon counting module, our overall collection efficiency is 0.45%. After correcting for the SSPD efficiency (≃40%), beam splitter (80%), and polarizer (50%) losses as well as the fiber coupling efficiency (40%), we conclude that 7.0% of the photons emitted by the QD are collected by the objective.

Figure 2 summarizes the experiments demonstrating single-shot spin readout on submicrosecond time scales. With the pulse sequence depicted in Fig. 1, we record time-resolved RF from the QD. Figure 2(a) shows the average RF counts, which decay exponentially during each pulse due to spin pumping [10]. By comparing the counts at the beginning and the end of laser 1 (2) pulse that is resonant with the vertical blue (red) transition, we estimate a lower bound of the spin-pumping fidelity $96.1\% \pm 1.0\%$ ($96.0\% \pm 0.7\%$) for $|\uparrow\rangle$ ($|\downarrow\rangle$) state. The imperfect spin pumping is mostly due to the off-resonant excitation of the other vertical transition and the finite pulse duration.

We remark that the detected RF signal in the second pulse for measuring $|\downarrow\rangle$ is higher than that in the first pulse as a consequence of the polarization settings in our system. In Faraday geometry, the two vertical cycling transitions $|\downarrow\rangle \leftrightarrow |T_r\rangle$ and $|\uparrow\rangle \leftrightarrow |T_b\rangle$ have equal oscillator strengths and are σ^- and σ^+ circularly polarized, respectively. We set the polarization of both lasers to be $\alpha\sigma^+ + \beta\sigma^-$. To suppress the reflected laser background, the polarizer in the collection arm is set so that it transmits $\alpha^*\sigma^- - \beta^*\sigma^+$ polarized light. In the limit $|\alpha| > |\beta|$, the detected σ^- RF counts will be larger by a factor $|\alpha|^2/|\beta|^2$, provided that we increase the intensity of laser 2 to ensure that the $|\downarrow\rangle \leftrightarrow |T_r\rangle$ transition is driven to saturation. From the total photon numbers in each pulse, we obtain $\alpha^2/\beta^2 = 2.60 \pm 0.01$ for our experiment.

Before describing our principal experimental observations, we argue that a natural definition of a single-shot measurement is provided by a comparison between the average waiting time t_{wait} between two successive photon detection events and the spin-flip time t_{spin}. We refer to the readout procedure as "single shot" if $t_{\text{wait}} \leq t_{\text{spin}}$; in this

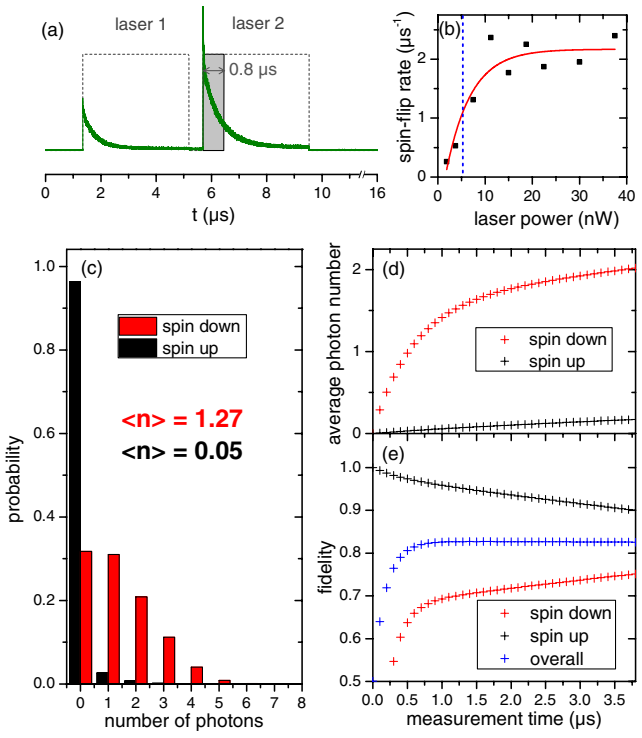

FIG. 2 (color online). (a) The time-resolved average RF counts measured with two lasers as shown in the energy level diagram in Fig. 1(c). The time range used to calculate the photon number probability in (c) is shown in the grey area. (b) Spin-flip rate as a function of the excitation laser power in the readout pulse. The saturation power is indicated by the dashed blue line. The error bars are smaller than the symbols, and the deviation from the exponential shape (red line) comes from laser-power-dependent dynamical nuclear spin polarization effects. (c) The normalized probability of photon number detected in a time range of 800 ns after the spin is prepared to the $|\uparrow\rangle$ (black column) or $|\downarrow\rangle$ (red column). The statistics are obtained from data in 10 seconds (618 000 repetitions). (d) The average number of detected photons for spin-up and spin-down state as a function of the readout duration. (e) The probability of detecting spin up and spin down, and the overall fidelity as a function of the readout duration. The error bar is smaller than the symbols.

limit we detect (on average) ≥ 1 photons before the spin flips from the bright state to the dark state [13]. As we discuss shortly, the time constants t_{wait} and t_{spin} emerge naturally in waiting time distribution $W(\tau)$ and second-order correlation function $g^{(2)}(\tau)$.

To perform a single-shot spin measurement, we prepare the spin state with laser 1 either in $|\uparrow\rangle$ or $|\downarrow\rangle$; afterwards, the spin state $|\downarrow\rangle$ is read out with laser 2 that is kept on resonance with $|\downarrow\rangle \leftrightarrow |T_r\rangle$ and its power is chosen to be 22 nW, about 4 times the saturation power [Fig. 2(b)]. Figure 2(c) shows the probability distribution of the photon counts in the first 800 ns of the readout pulse, corresponding to the grey time window in Fig. 2(a). When the spin state is prepared by laser 1 in $|\uparrow\rangle$, detecting zero photons is the most likely outcome. Conversely, for the spin prepared in $|\downarrow\rangle$, it is more likely that one or more photons are detected. We find that in this latter case, the average number of detected photons is 1.27 ± 0.01, demonstrating single-shot measurement of the electron spin state. The deviation of the detected photon number distribution from a geometric distribution is mainly due to the dead time of our time-correlated single photon counting module (~90 ns) and the size of the detection window which is comparable to the spin lifetime.

When the initial state is $|\downarrow\rangle$, the average detected photon number $\langle n \rangle$ increases with a larger detection window, mainly due to incomplete spin pumping in the first 800 ns depicted in Fig. 2(c). For a detection window of 3.8 μs, $\langle n \rangle$ is increased to ~2 [Fig. 2(d)]. For $|\uparrow\rangle$, the average counts will also increase with increasing measurement or recording time to 0.1; these counts stem primarily from the residual reflected laser photons. In the spin-state measurement, if we detect no photons, we assign the spin state as $|\uparrow\rangle$. If on the other hand, we detect one or more photons, we assign the spin state prior to the measurement pulse as $|\downarrow\rangle$. The average spin readout fidelity $F_{\text{avg}} = 1/2(p_{|\uparrow\rangle} + p_{|\downarrow\rangle})$ we measure is 0.823 ± 0.002 for a detection window of 800 ns and 0.826 ± 0.002 for a detection window of 3.8 μs. Here $p_{|\uparrow\rangle}$ is the probability of detecting no photons when the initial spin state is $|\uparrow\rangle$; $p_{|\downarrow\rangle}$ denotes the probability that at least one photon is detected when the initial state is $|\downarrow\rangle$).

Single-shot readout capability enables the observation of quantum jumps in spin dynamics. In our experiments, the changes in the spin state are predominantly due to spin-flip Raman scattering processes. To observe the associated spin jumps, we choose a two laser excitation configuration depicted in Fig. 1(d). A strong cw laser resonant with the red vertical transition is used to detect the $|\downarrow\rangle$ state while inducing spin pumping into $|\uparrow\rangle$. A second cw laser resonant with the diagonal transition is used for inducing spin flips from $|\uparrow\rangle$ back to $|\downarrow\rangle$. The intensity of the lasers are chosen to ensure a spin-pumping (repumping) time ~1 μs (~10 μs). The photon detection events are shown in Fig. 3(a) for a detection time window of 100 μs, for two different values P_a and P_b of the repumping laser power: the registred detection events bunch together into separated clusters, showing alternating bright and dark periods that indicate jumps in the electron spin state.

In order to extract the characteristic constants of the spin dynamics from the continuous measurement time traces, we calculate the functions $g^{(2)}(\tau)$ (second-order correlation function) and $W(\tau)$ (waiting time distribution) from the experimental data. The unnormalized $g^{(2)}(\tau)$ curve, obtained from 1-s-long RF traces, is shown in Fig. 3(c). The bunching behavior reveals information about the spin-flip dynamics. An exponential decay fit to the $g^{(2)}(\tau)$ curve gives a spin lifetime of $t_{\text{spin}} = 972 \pm 4$ ns. Using the same data, we also determine $W(\tau)$, which gives, conditional on detecting one photon, the probability of detecting a second

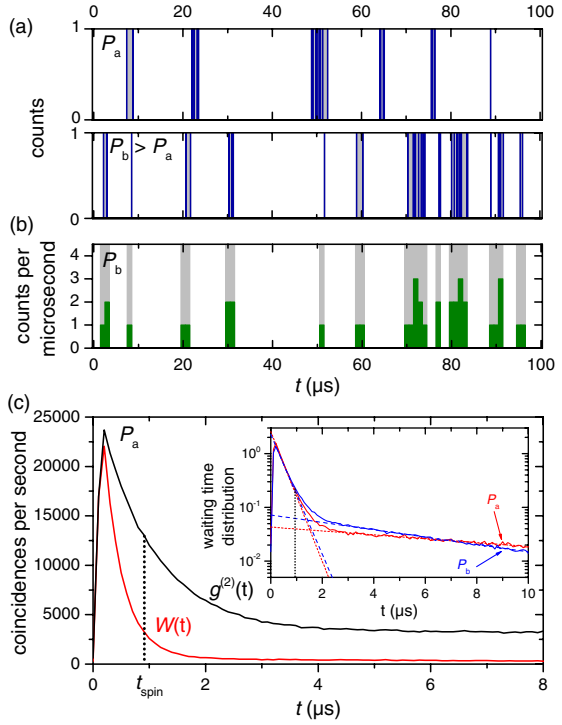

FIG. 3 (color online). (a) Quantum jumps in continuous readout. The power of laser used for exciting the diagonal transition is weaker for the upper panel (P_a) and stronger for the lower panel ($P_b > P_a$). (b) Same data as (a), lower panel, but the counts are stored in 1 μs bins. (c) Second-order correlation function $g^{(2)}(t)$ (black trace) and waiting time distribution (red trace) for the data in the upper panel of (a). The dashed line shows the spin lifetime. Inset: the normalized waiting time function for the upper panel (red line) and the lower panel (blue line) in (a). Two exponential decays are observed. The fitted decay times for the red line are $t_{\text{wait}} = 349 \pm 5$ ns and $t_{\text{repump}} = 12.1 \pm 0.3$ μs and for the blue line $t_{\text{wait}} = 371 \pm 5$ ns and $t_{\text{repump}} = 6.32 \pm 0.07$ μs.

photon after a waiting time τ without any detection event in between [red curve in Fig. 3(c)]. The construction of $g^2(\tau)$ and $W(\tau)$ is discussed in more detail in the Supplemental Material [14]. In the inset of the Fig. 3(c), the normalized $W(\tau)$ is shown in log scale for two different values of the diagonal repumping laser power. Two exponential decays can be observed [7,8]: the first one with a time-constant t_{wait} stems from the detection of the second photon while the spin state remains the same. The much longer second decay time (t_{repump}) originates from the cases where two consecutive spin flips take place in between two detection events; thus, t_{repump} strongly depends on the repumping laser power, whereas t_{wait} is independent of it. This allows us to write $W(\tau)$ as the sum of these two exponential contributions, namely $W(\tau) = W_{\text{short}}(\tau) + W_{\text{long}}(\tau)$, where $W_{\text{short}}(\tau)$ [$W_{\text{long}}(\tau)$] is the component with the short (long) decay time constant t_{wait} (t_{repump}). The low value of both $g^{(2)}(\tau = 0)$ and $W(\tau = 0)$ is caused by the dead time of our time-correlated single photon counting module and does not correspond to the actual physical value of these functions for $\tau = 0$. The fact that $W(\tau)$ does not present sizable deviation from the biexponential shape indicates that the dynamics of our system in the considered time scales can be treated incoherently using rate equations [8].

The three time constants, namely t_{spin}, t_{wait} and t_{repump}, are the relevant quantities in the following analysis of quantum jumps. The observation of quantum jumps requires the fulfillment of two conditions: first, t_{spin} should be longer than t_{wait} in order to detect a significant number of photons when the spin is in the $|\downarrow\rangle$ state. This condition is equivalent to the single-shot readout condition, which is satisfied in our experiments. Second, t_{repump} has to be much longer than t_{wait} in order to make a clear distinction between waiting events occurring while the spin remains in the $|\downarrow\rangle$ state, and longer waiting events associated with two consecutive spin-flip processes. These conditions lead to a binary RF signal, presenting alternating bright and dark periods with abrupt changes [15,16]. From the fits depicted in Fig. 3(c), we find in our case $t_{\text{repump}} > t_{\text{spin}} > t_{\text{wait}}$, allowing the observation of quantum jumps. To identify a waiting period $(t_1, t_1 + \tau)$ between two consecutive photon detection events as bright or dark, we use $W(\tau)$: if $W_{\text{short}}(\tau) > W_{\text{long}}(\tau)$ ($W_{\text{short}}(\tau) < W_{\text{long}}(\tau)$), then we identify the period $(t_1, t_1 + \tau)$ as a bright (dark) period and shade it in Fig. 3(a) in grey (white).

A direct distinction between these waiting events of very different origins can be made as well by binning the data with a judicious choice of the bin size T_{bin}, such that $t_{\text{repump}} \gg T_{\text{bin}} > t_{\text{wait}}$. In this case, the short waiting events are integrated in the bins: a change in n for two consecutive bins from $n \geq 1$ to $n = 0$ identifies a quantum jump. Figure 3(b) presents the same data as in the lower panel of Fig. 3(a), with the counts integrated into 1 μs bins. The inferred bright periods are in excellent agreement with the identification based on comparing $W_{\text{short}}(\tau)$ and $W_{\text{long}}(\tau)$, depicted in the lower panel of Fig. 3(a). The dark periods dominate over the bright periods since we have set $t_{\text{repump}} > t_{\text{spin}}$.

In summary, we report the observation of submicrosecond all-optical single-shot measurement of an isolated electron spin confined in a single quantum dot. We expect this result to stimulate research aimed at probabilistic entanglement of distant spins which have so far been hindered by inefficient multishot spin measurements. Embedding a quantum dot in a photonic nanostructure could be used to enhance the collection efficiency by a factor of 10 [17]. Together with a Purcell enhancement factor $F_p \sim 4$ [17], the measurement could be achieved within 20 nanoseconds with a fidelity of 95%. We emphasize in addition that the characterization of spin jumps using the waiting time distribution shows the power of quantum optical measurements in identifying the elementary properties of optically active solid-state qubits.

This work is supported by NCCR Quantum Science and Technology (NCCR QSIT), a research instrument of the

Swiss National Science Foundation (SNSF), by the Swiss NSF under Grant No. 200021-140818, an ERC Advanced Investigator Grant (A. I.). The research leading to these results has received funding from the European Union Seventh Framework Programme (FP7/2007-2013) under Grant Agreement No. 289795. A. D. and W.-B. G. contributed equally to this work.

[1] D. P. DiVincenzo, Fortschr. Phys. **48**, 771 (2000).
[2] J. Elzerman, R. Hanson, L. H. Willems van Beveren, B. Witkamp, L. M. K. Vandersypen, and L. P. Kouwenhoven, Nature (London) **430**, 431 (2004).
[3] A. Morello *et al.*, Nature (London) **467**, 687 (2010).
[4] L. Robledo, L. Childress, H. Bernien, B. Hensen, P. F. A. Alkemade, and R. Hanson, Nature (London) **477**, 574 (2011).
[5] A. N. Vamivakas, C.-Y. Lu, C. Matthiesen, Y. Zhao, S. Fält, A. Badolato, and M. Atatüre, Nature (London) **467**, 297 (2010).
[6] C.-Y. Lu, Y. Zhao, A. N. Vamivakas, C. Matthiesen, S. Fält, A. Badolato, and M. Atatüre, Phys. Rev. B **81**, 035332 (2010).
[7] C. Cohen-Tannoudji and J. Dalibard, Europhys. Lett. **1**, 441 (1986).
[8] P. Zoller, M. Marte, and D. F. Walls, Phys. Rev. A **35**, 198 (1987).
[9] S. T. Yilmaz, P. Fallahi, and A. Imamoğlu, Phys. Rev. Lett. **105**, 033601 (2010).
[10] M. Atatüre, J. Dreiser, A. Badolato, A. Högele, K. Karrai, and A. Imamoğlu, Science **312**, 551 (2006).
[11] X. Xu, Y. Wu, B. Sun, Q. Huang, J. Cheng, D. G. Steel, A. S. Bracker, D. Gammon, C. Emary, and L. J. Sham, Phys. Rev. Lett. **99**, 097401 (2007).
[12] C. Latta *et al.*, Nat. Phys. **5** 758 (2009).
[13] Note that the presence of a dead time in the detection apparatus will decrease the average photon number but not the measurement fidelity as it affects only the situations involving at least one detection event.
[14] See Supplemental Material at http://link.aps.org/supplemental/10.1103/PhysRevLett.112.116802 for more detail about the construction of the functions $g^2(\tau)$ and $W(\tau)$.
[15] W. Nagourney, I. Sandberg, and H. Dehmelt, Phys. Rev. Lett. **56**, 2797 (1986).
[16] T. Sauter, W. Neuhauser, R. Blatt, and P. E. Toschekt, Phys. Rev. Lett. **57**, 1696 (1986).
[17] O. Gazzano, S. Michaelis de Vasconcellos, C. Arnold, A. Nowak, E. Galopin, I. Sagnes, L. Lanco, A. Lemaître, and P. Senellart, Nat. Commun. **4**, 1425 (2013).